



OPEN

Impact of surface treatments on the photocatalytic performance of anodic aluminum oxide templates

Carina Hedrich^{1,2}, Robin R. Petit³, Matthias M. Minjauw³, Anna R. Burson¹, Stefanie Haugg¹, Kaline P. Furlan^{2,4}, Christophe Detavernier³, Jolien Dendooven³, Robert H. Blick¹ & Robert Zierold¹✉

Nanostructured materials receive great interest nowadays due to their unique properties, increased surface areas, and superior performances with associated reduced material usage. However, directly nanostructuring functional materials themselves can be technologically challenging. Hence, nanostructured substrates such as anodic aluminum oxide (AAO) can serve as templates for depositing active materials. The templates' chemical stability is crucial for accurately assessing functional materials. Since AAO structures incorporate electrolyte ions during anodization, their chemical stability is influenced by the subsequent processing after anodization. This work investigates the effect of various post-anodization modifications on the surface chemistry and photocatalytic performance of bare AAO structures. Treatments with H_2O_2 or H_3PO_4 can stabilize the photocatalytic performance of the AAO templates over consecutive measurements. XPS measurements indicate that such stabilization results from AAO surface chemistry alterations. Further, we explore the functionalization of these modified AAO templates with photocatalysts by atomic layer deposition. The photocatalytic performance of TiO_2 as a chemically stable photocatalyst is not affected by the templates' post-anodization treatment. In contrast, the performance of templates functionalized with Fe_2O_3 as an inherent chemically unstable photocatalyst depends on the template stability. This work highlights the importance of chemically stable template materials for exploring the properties of new functional materials.

Keywords Anodic aluminum oxide, Photocatalysis, Surface chemistry, XPS, Nanostructured templates

Achieving high functionality while minimizing material usage is a pivotal aim in materials science^{1,2}. Nanostructuring has emerged as a key strategy to meet this goal, enabling the tailoring of materials at the nanoscale to expand their functionalities^{2,3}. Moreover, nanostructuring leads to significantly enlarged surface areas while the material usage is simultaneously reduced²⁻⁵. Accordingly, nanostructured materials are often utilized either directly or as templates for electronics, photonics, (photo-)catalysis, biomedicine, energy storage and conversion, environmental applications, and magnetic devices^{2,3,6-8}. To identify the properties of functional materials deposited onto nanostructured templates, it is crucial to use a chemically stable structure as template^{9,10}. Specifically, the template should not decompose or undergo any other chemical changes during the applications as it will be functionalized with an active material.

One prominent example of such nanostructured templates is anodic aluminum oxide (AAO) which has been used for many different applications such as optics, sensing, catalysis, energy storage, or electronics over the past years^{6,11-14}. AAO consists of cylindrical pores inside an aluminum oxide (Al_2O_3) matrix produced by an electrochemical oxidation also known as anodization¹³. The pores are highly ordered in a hexagonal pattern due to a self-assembly process and are aligned perpendicular to the surface^{8,15}. AAO provides a large flexibility as template structure, because the pore size, pore morphology, layer thickness, and surface functionalization can be widely tailored during or after the anodization^{6,13,14}. Furthermore, due to the porous nature, AAO templates feature high surface areas which are beneficial for many applications, e.g., photo(electro)catalysis, solar cells, and

¹Center for Hybrid Nanostructures, Universität Hamburg, Luruper Chaussee 149, 22761 Hamburg, Germany.

²Integrated Ceramic-based Materials Systems Group, Hamburg University of Technology (TUHH), Denickestraße 15, 21073 Hamburg, Germany. ³CoCoN Group, Department of Solid State Sciences, Ghent University, Krijgslaan 281/S1, 9000 Ghent, Belgium. ⁴ Karlsruhe Institute of Technology (KIT), Institute for Applied Materials – Ceramic Materials and Technologies (IAM-KWT), Haid-und-Neu-Strasse 7, 76131 Karlsruhe, Germany. ✉email: robert.zierold@uni-hamburg.de

batteries^{6,7,14,16}. However, anodization is accompanied by contamination of the aluminum oxide matrix by the formation of oxygen vacancies in the aluminum oxide and through the incorporation of anions of the utilized acidic electrolyte^{17–21}. The contamination percentage is increasing from the inner side of the pores towards the outer part, i.e., the one in contact with the electrolyte during anodization as schematically shown in Fig. 1. These contaminations are inevitable and they can cause undesired properties of the AAO template such as high photoluminescence activity^{20–24}. Moreover, these contaminations could be dissolved when exposed to or reacted with aqueous solutions which are applied, for example, to functionalize the AAO surface. Consequently, such dissolution processes may alter the intrinsic properties of AAO as a template material. Furthermore, besides chemical impurities, oxygen vacancies present in the AAO matrix are also known to cause photoluminescence of the structure^{20–22,24,25}. Healing of these defects can be attempted by tailored annealing processes. Note, since AAO often serves as a template structure and thus is coated with functional materials, it is essential that the alumina surface is stable against the required treatments^{8,26,27}. On the one hand, the surface chemistry has to be modified by depositing a material of choice onto the AAO template. On the other hand, the surface chemistry should not be altered in a way that affects the properties of the AAO template structure. Chemically stable templates non-interacting with the coating allow for investigating functional materials – even those which are prone to decompose during their application. The influence of AAO's surface chemistry onto its applicability as template structure can for example be studied for photocatalytic applications. Photocatalysis is based on the induction of chemical reactions by irradiation with light and it offers a plethora of possible applications such as water or air purification, hydrogen production, self-cleaning surfaces, or energy conversion^{4,28–32}. Since photocatalytic reactions occur at the surface of materials, an increment of the surface area corresponds to an increase of the reactions per time period potentially leading to a more efficient process^{4–5}. Thus, AAO structures are a great choice of template structure for photocatalysts due to their high surface area, scalable and comparably inexpensive fabrication, and versatile functionalization possibilities.

This study explores the influence of different post-anodization treatments of AAO templates on their properties with the main goal of obtaining a stable and robust surface chemistry for the exemplary application of photocatalysis. Post-anodization treatments – namely immersion in hydrogen peroxide (H_2O_2) and immersion in phosphoric acid (H_3PO_4) – are applied prior to functionalization with titanium dioxide (TiO_2) or iron (III) oxide (Fe_2O_3) as a photocatalyst by atomic layer deposition (ALD) and are compared to as-prepared AAO templates functionalized with the respective photocatalyst. Due to sequential, self-limiting reactions between precursors

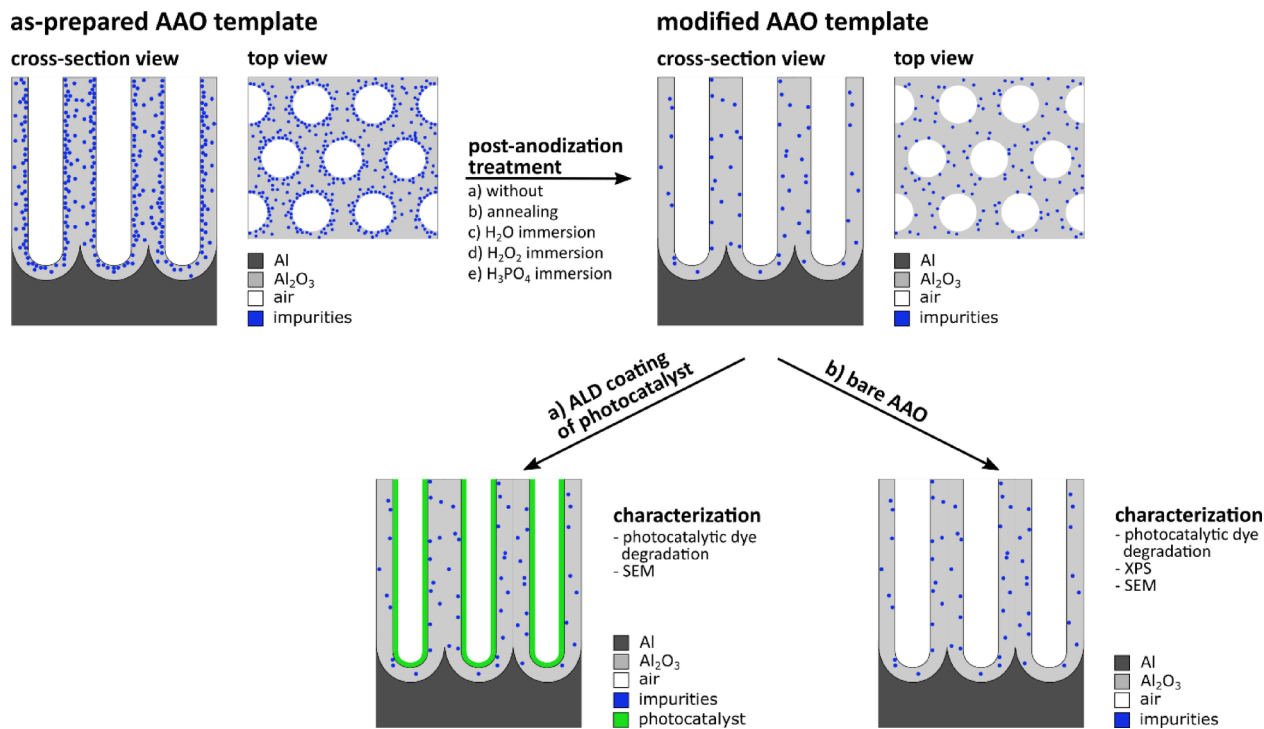


Fig. 1. Schematic illustration of the AAO template structure, processing, and characterization. As-prepared AAO templates contain electrolyte impurities in their Al_2O_3 matrix. The impurities are incorporated during fabrication and their concentration is increasing from the Al_2O_3 matrix towards the Al_2O_3 /air interfaces, i.e., the interfaces in contact with the electrolyte during anodization. Herein, post-anodization treatments are applied to modify the AAO templates' surface chemistry by (partially) removing the impurities. The photocatalytic performance of (a) modified AAO templates with photocatalyst ALD coating and of (b) modified bare AAO templates is assessed by dye degradation. Moreover, the influence of the different post-anodization treatments on the surface chemistry of the AAO templates is characterized by X-ray photoelectron spectroscopy (XPS).

in the gas phase, and solid substrate surfaces, ALD allows for complete conformal coating of the substrate – here AAO – while simultaneously controlling the deposited film thickness in the sub-nanometer range^{33–36}. TiO₂-coated structures showed stable photocatalytic performances over three measurements for all investigated post-anodization modifications, suggesting little to no influence by the post-anodization treatments. In contrast, the photocatalytic activity of Fe₂O₃-functionalized samples is stable for AAO templates immersed in H₂O₂ or H₃PO₄ but decreases within the subsequent measurements for the as-prepared AAO template. This observed behavior is probably caused by modifications of the AAO surface chemistry depending on the respective post-anodization treatment. To reveal the influence of the surface treatments on the photocatalytic properties, the photocatalytic performances of bare post-anodization modified AAO templates without additional ALD coating (Fig. 1) were investigated. Furthermore, additional surface modifications were tested. In detail, immersion of AAO templates into water (H₂O), H₂O₂, or H₃PO₄, and thermal annealing are applied as post-anodization treatments and compared to an as-prepared AAO template. The effect of the different modifications on the AAO surface chemistry is examined by X-ray photoelectron spectroscopy (XPS). The results obtained in this work shed light on modifying the surface properties of AAO templates driven by post-anodization modifications.

Results and discussion

Properties of ALD-functionalized AAO

Highly ordered AAO structures featuring a pore length of about 30 µm and a pore diameter of 25 nm were fabricated by anodization. Herein, the photocatalytic performance of post-anodization treated AAO templates is assessed by the degradation of MB as a model pollutant of water. ALD-coating of photocatalyst materials onto AAO templates exposed to hydrogen peroxide (H₂O₂) or phosphoric acid (H₃PO₄) after the anodization reveals the importance of the post-anodization treatment for the photocatalytic performance and stability of the photocatalyst. On the one hand, a chemically stable photocatalyst – here TiO₂ – is not significantly affected by the post-anodization treatment. On the other hand, an inherent chemically unstable photocatalyst – here Fe₂O₃ – is known to get degraded through redox reactions and photocorrosive processes and shows decreasing performance over subsequent measurements. Note, the as-deposited ALD-grown TiO₂ and Fe₂O₃ films are amorphous and are used without further modification to prevent additional effects on the AAO template structure.

TiO₂-functionalized structures presented stable photocatalytic properties regardless the surface treatment as depicted in Fig. 2a. The 5 nm thick amorphous TiO₂ coatings deposited onto the AAO templates are chemically very stable and thus, it is expected that they are not strongly influenced by the underlying template³⁷. Fig. 2a shows stable photocatalytic activities of TiO₂-functionalized AAO templates during three consecutive measurements for all three investigated templates, namely as-prepared AAO, H₂O₂-treated AAO, and H₃PO₄-treated AAO. The mean activities of as-prepared and H₂O₂-treated samples are very similar ($1.18 \pm 0.05 \text{ h}^{-1}$ and $1.17 \pm 0.04 \text{ h}^{-1}$). However, the structure immersed in H₃PO₄ solution features a lower photocatalytic activity of $1.04 \pm 0.02 \text{ h}^{-1}$. The reasons for this behavior are discussed in details when presenting the XPS measurements.

Meanwhile, the photocatalytic performance of 5 nm amorphous Fe₂O₃-functionalized AAO shows a strong dependence on the post-anodization treatment as shown in Fig. 2b. We exclude photocorrosion of the Fe₂O₃ layer as a possible explanation since an ultra-thin Al₂O₃ coating of 2 ALD cycles was deposited onto the structures³⁸. By analyzing and comparing the data from Fe₂O₃ to TiO₂, three key findings have been revealed: First, the photocatalytic performance of Fe₂O₃-functionalized AAO is very stable over three measurements for structures treated with H₂O₂ or H₃PO₄ featuring mean activities of $1.16 \pm 0.02 \text{ h}^{-1}$ and $1.30 \pm 0.04 \text{ h}^{-1}$, respectively. In contrast, a strong decrease of the activity after the first measurement is observed for an as-prepared AAO

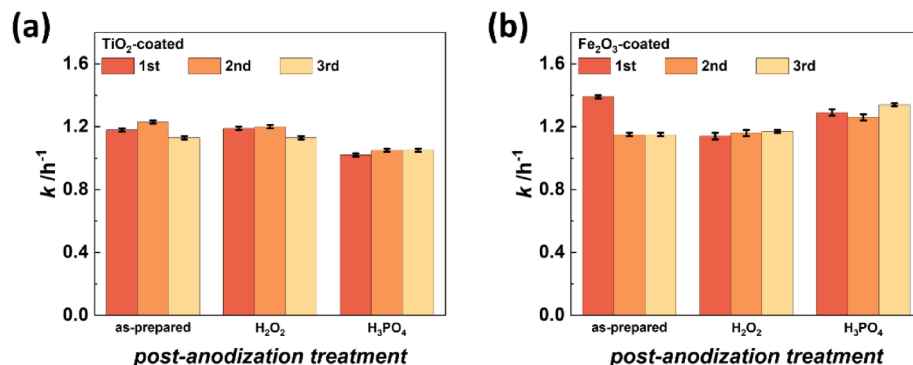


Fig. 2. Photocatalytic performances of post-anodization modified AAO templates that were afterwards coated with a photocatalyst by ALD. (a) TiO₂-functionalized samples show stable photocatalytic activities for all three post-anodization treatments over three consecutive measurements. The mean photocatalytic activities are $1.18 \pm 0.05 \text{ h}^{-1}$, $1.17 \pm 0.04 \text{ h}^{-1}$, and $1.04 \pm 0.02 \text{ h}^{-1}$ for as-prepared, H₂O₂-treated, and H₃PO₄-treated templates, respectively. (b) Coating Fe₂O₃ as a chemically less stable photocatalyst onto AAO templates demonstrates a dependence of the photocatalytic performance stability on the previously applied treatment. The Fe₂O₃-coated templates feature mean activities of $1.23 \pm 0.14 \text{ h}^{-1}$ (as-prepared), $1.16 \pm 0.02 \text{ h}^{-1}$ (H₂O₂-treated), and $1.30 \pm 0.04 \text{ h}^{-1}$ (H₃PO₄-treated).

template. This performance loss resembles in a high standard deviation ($1.23 \pm 0.14 \text{ h}^{-1}$). Second, and at the same time, the mean activity for H_3PO_4 -treated AAO functionalized with Fe_2O_3 is significantly higher than for a treatment with H_2O_2 . Third, this observation is in contrast to the TiO_2 -coated AAOs, where the H_3PO_4 -treatment reveals the lowest activity.

Electrolyte ions present in the Al_2O_3 matrix of the as-prepared AAO can potentially react with the surface when activated by charge carriers of the photocatalytic processes. In this way, the photocatalyst is chemically altered and the photocatalytic activity is influenced. EDX measurements of the TiO_2 -coated AAO templates demonstrated an almost constant Ti content independent of the surface treatment before ALD (Table S1) proving that the influence of the surface treatment onto the TiO_2 ALD process is negligible. Due to charging effect, measurement of iron oxide was not straight forward, but we do not foresee any influence of the treatments onto the ALD growth. XPS measurements of the ALD-grown photocatalysts are shown in Figure S1. For the TiO_2 -functionalized AAO structure, the $\text{Ti}_{2\text{p}3/2}$ peak and the $\text{Ti}_{2\text{p}1/2}$ peak feature a spin-orbit splitting of 5.7 eV indicating the Ti(IV) oxidation state which is present in TiO_2 ^{39,40}. Moreover, based on the survey spectrum, the atomic percentages for Ti and O are present with the expected ratio for TiO_2 , when taking into account the O-bonds with C and Al. The $\text{Fe}_{2\text{p}3/2}$ peak and the $\text{Fe}_{2\text{p}1/2}$ peak of the Fe_2O_3 -coated AAO structure are separated by 13.2 eV. In combination with the $\text{Fe}_{2\text{p}3/2}$ peak position at a binding energy (B.E.) of 711 eV, low satellite peak intensities and the atomic percentages for Fe and O, such features were previously assigned to the Fe_2O_3 phase⁴¹.

The applied surface treatments and ALD coating did not influence the morphology of the straight pores of the AAO templates as depicted in the cross-section scanning electron microscope (SEM) images in Figure S2. Further, no morphology changes are observed when comparing the samples before and after the photocatalysis measurements. Top-view SEM images in Figure S3 confirm that the ALD-coated AAO templates do not present a visible change in the pore morphology or film structure before and after photocatalysis tests. Note that exploring new photocatalytic or other functional materials coated onto AAO templates necessitates a chemically stable and known template to accurately characterize the materials' properties. Hence, we studied the influence of common post-anodization treatments on the photocatalytic performance of AAO templates to obtain a more detailed understanding of the surface chemistry changes which do not affect the pore morphology.

Effect of post-anodization surface treatments on AAO templates

The influence of four different post-anodization treatments of AAO templates on their photocatalytic performance is investigated to identify treatments which stabilize the AAO properties. Taking frequently reported treatments of AAO templates such as pore diameter modifications into account, we assessed the effects of AAO thermal annealing, and immersion into H_2O , H_2O_2 , or H_3PO_4 compared to an as-prepared AAO template. As depicted in Fig. 1, these templates are referred to as bare AAO templates since they were exposed to post-anodization treatments but no further coating was applied. As reference, the obtained photocatalytic activity of a blank measurement (without sample) and a 20 nm Al_2O_3 -coated planar Si wafer are shown in Figure S4. The presence of H_2O_2 in the analyte solution can also contribute to direct photolysis of MB. Hence, a low MB degradation rate of $0.52 \pm 0.01 \text{ h}^{-1}$ is observed even when no samples is tested. While the photocatalytic activity is decreasing for an as-prepared and annealed AAO template (Fig. 3) within three consecutive measurements ($1.05 \pm 0.12 \text{ h}^{-1}$ and $0.93 \pm 0.16 \text{ h}^{-1}$, respectively), it can be stabilized by certain wet-chemical post-anodization treatments. Decreasing photocatalytic activities in consecutive measurements are typically caused by the change of the chemical state of the structures' surface or by structural decomposition^{42–44}. Since Al_2O_3 is a chemically and temperature stable material and no additional photocatalyst material is applied here, saturation or removal of contamination electrolyte ions are possible reasons for the decreasing activity. These species provide unsaturated sites within the alumina matrix and can therefore lead to undesired side-reactions where they react with other compounds or they can potentially be removed from the structure by dissolution in aqueous media⁴⁵. The side-

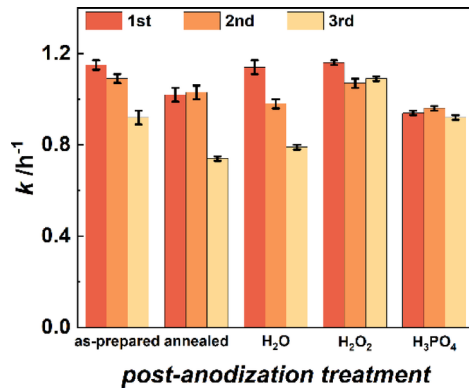


Fig. 3. Photocatalytic performances of post-anodization modified AAO templates. The photocatalytic activities remain constant or decrease over three consecutive measurements depending on the applied treatment. Differences in the stability of the photocatalytic performances are also reflected in the mean value and standard deviation of the activity k . The modified templates feature the following mean activities: $1.05 \pm 0.12 \text{ h}^{-1}$ (as-prepared), $0.93 \pm 0.16 \text{ h}^{-1}$ (annealed), $0.97 \pm 0.18 \text{ h}^{-1}$ (H_2O -treated), $1.11 \pm 0.05 \text{ h}^{-1}$ (H_2O_2 -treated), and $0.98 \pm 0.02 \text{ h}^{-1}$ (H_3PO_4 -treated).

reactions occur until all accessible contaminations have either reacted to stable species or are removed from the Al_2O_3 matrix, for example by dissolving them in a pore filling medium. The H_2O -treated AAO template exhibits a clearly decreasing photocatalytic activity within consecutive measurements as also indicated by an increased standard deviation ($0.97 \pm 0.18 \text{ h}^{-1}$). In contrast, AAO templates immersed in H_2O_2 for 24 h or in H_3PO_4 for 1 min show the most stable photocatalytic performance over three measurements. Although the activity variation is slightly larger for the H_2O_2 -treated samples ($1.11 \pm 0.05 \text{ h}^{-1}$) than for the H_3PO_4 -treated sample ($0.98 \pm 0.02 \text{ h}^{-1}$), its mean activity is higher.

The different absolute photocatalytic activities are hypothesized to originate from the different surface chemistry after post-anodization treatments. Our observation is in agreement with similar results which have previously been reported for TiO_2 nanoparticles and for anodized TiO_2 ^{45,46}. Hence, we investigated the surface chemistry variations in detail with XPS measurements of the AAO structures after post-anodization treatments. The identified peak positions for all samples are summarized in Table S2 in the Supporting Information and the data analysis parameters are listed in Table S3. These XPS measurements demonstrate changes of the present surface groups and their ratios depending on the respective post-anodization treatment (Fig. 4). The as-prepared AAO template (Fig. 4a) features Al_2O_3 , Al-OH groups, and O-Al-O bonds at the Al_{2p} peak corresponding to the Al_2O_3 matrix and expected hydroxy groups at the surface⁶. Different types of carbon-carbon and carbon-hydrogen bonds, carbon-oxygen bonds, and carbon-fluor bonds can be identified at the C_{1s} peak. The carbon-carbon and carbon-oxygen bonds are probably caused by incorporated oxalate ions. These ion species originate from the inherent structure of the produced AAO, i.e., electrolyte ions built into the aluminum oxide during the anodization process^{13,19}. Hence, O-C=O, C-C, and C-H bonds at the AAO surface identified by the XPS measurements can be attributed to residues of oxalic acid ($\text{H}_2\text{C}_2\text{O}_4$) which was used as electrolyte during the anodization process. For the O_{1s} peak of the as-prepared structure, Al_2O_3 bonds, OH groups, and COOH groups and adsorbed water molecules are observed. Note that for all discussed peaks, some bonds cannot be distinguished as their B.E.s are too close to each other. XPS survey spectra of the AAO templates modified with different surface treatments are depicted in Figure S5.

Post-anodization treatments can reduce the amount of contaminations as revealed by the XPS spectra. Thermal annealing predominantly removes -OH groups, -O bonds, and adsorbed H_2O molecules from the surface as shown in Fig. 4b. Such behavior is in agreement with existing literature about the influence of annealing on the surface of Al_2O_3 ^{19,22,24}. Thermal annealing was previously reported of being capable to reduce photoluminescence intensities of AAO templates due to the thermal decomposition of the incorporated electrolyte ions and saturation of oxygen vacancies during the annealing^{22,24}. Such treatment affects the complete alumina matrix and thus, results in a large amount of electrolyte decomposition and vacancy saturation which can no longer contribute to photoluminescence-induced degradation of the dye. The -OH groups are not completely removed which might be caused by the comparable low annealing temperature of 450°C , since Han et al. reported that annealing temperatures of at least 500°C are necessary to remove -OH groups²⁴. Although the subpeaks of the C_{1s} peak and the Al-OH contents are reduced for the sample annealed at 450°C for 1 h, the photocatalytic activity could not be stabilized but instead shows a lower mean value. To prove further removal of -OH groups, oxalate incorporations, and carbon content, another AAO structure was annealed at 600°C for 1 h and characterized by XPS. The spectra shown in Figure S6 and summarized in Table S4 demonstrate a reduction of -OH groups, Al-O bonds, and C content compared to the AAO structure annealed at 450°C which is in good agreement to previous reports^{19,22,24}. Immersing AAO templates in aqueous media could potentially dissolve oxalate ions incorporated into the AAO structure during anodization. XPS spectra of the AAO template soaked in H_2O demonstrate a decreased Al-OH signal compared to the as-prepared sample (Fig. 4c). Moreover, the C-OH content and C-O bond signal are decreasing. Based on the XPS results, we assume that the H_2O post-anodization treatment dissolves oxalic acid molecules which might then partially react with the AAO surface to form Al-oxalate. It was previously reported that treatments in aqueous solutions can lead to the dissociation of incorporated electrolyte ions in anodized metal oxides⁴⁵. In this way, the amount of ions inside the AAO matrix in close vicinity to the surface gets reduced. A H_2O treatment might be capable of removing electrolyte ions from the alumina matrix by dissolution, but the ions then present in solution cannot be further decomposed or chemically bound. A significant decrease in the photocatalytic performance observed for the H_2O -immersed AAO templates over consecutive measurements could be caused by the partial dissolution of oxalate species from the matrix during the post-anodization treatment. Since these species could not be decomposed simply by the H_2O treatment, they might physisorb at the surface and could potentially contribute to the photocatalytic activity. However, they are degrading during the photocatalytic reaction resulting in decreasing activities with increasing measurement numbers.

If the aqueous solution contains oxidizing species such as hydrogen peroxide (H_2O_2), the removed electrolyte ions can immediately be further decomposed. The destruction of oxalate species by H_2O_2 results in the complete oxidation of the ions to carbon dioxide (CO_2)⁴⁷. As depicted in Fig. 4d, immersion of AAO into H_2O_2 removes Al-OH groups and especially Al-O bonds from the surface as indicated by the Al_{2p} peak profile. While the content of O-C=O groups slightly increases in the C_{1s} peak, the Al_2O_3 and OH group signals in the O_{1s} peak also increase. Here, the sub-peak of COOH groups/ adsorbed water molecules is no longer present. This indicates that incorporated oxalic acid species are likely dissolved by this treatment and could potentially react with Al-OH and Al-O groups at the surface to form stable Al-oxalate complexes explaining the increasing Al_2O_3 content. In addition, H_2O_2 could act as an electron acceptor and thus accelerate the formation of Al-oxalate. Further, the present OH-groups are mainly bound to oxalate species. The photocatalytic activity stabilization for the H_2O_2 treatment is probably caused by the saturation of surface groups and removal of electrolyte ions from the surface vicinity as observed in the XPS measurements. The proposed formation of Al-oxalate results in a stable surface chemistry which is not affected by the solution utilized in the photocatalysis measurements or the photocatalytic reactions themselves, also displayed in Fig. 3 by a high mean photocatalytic activity with

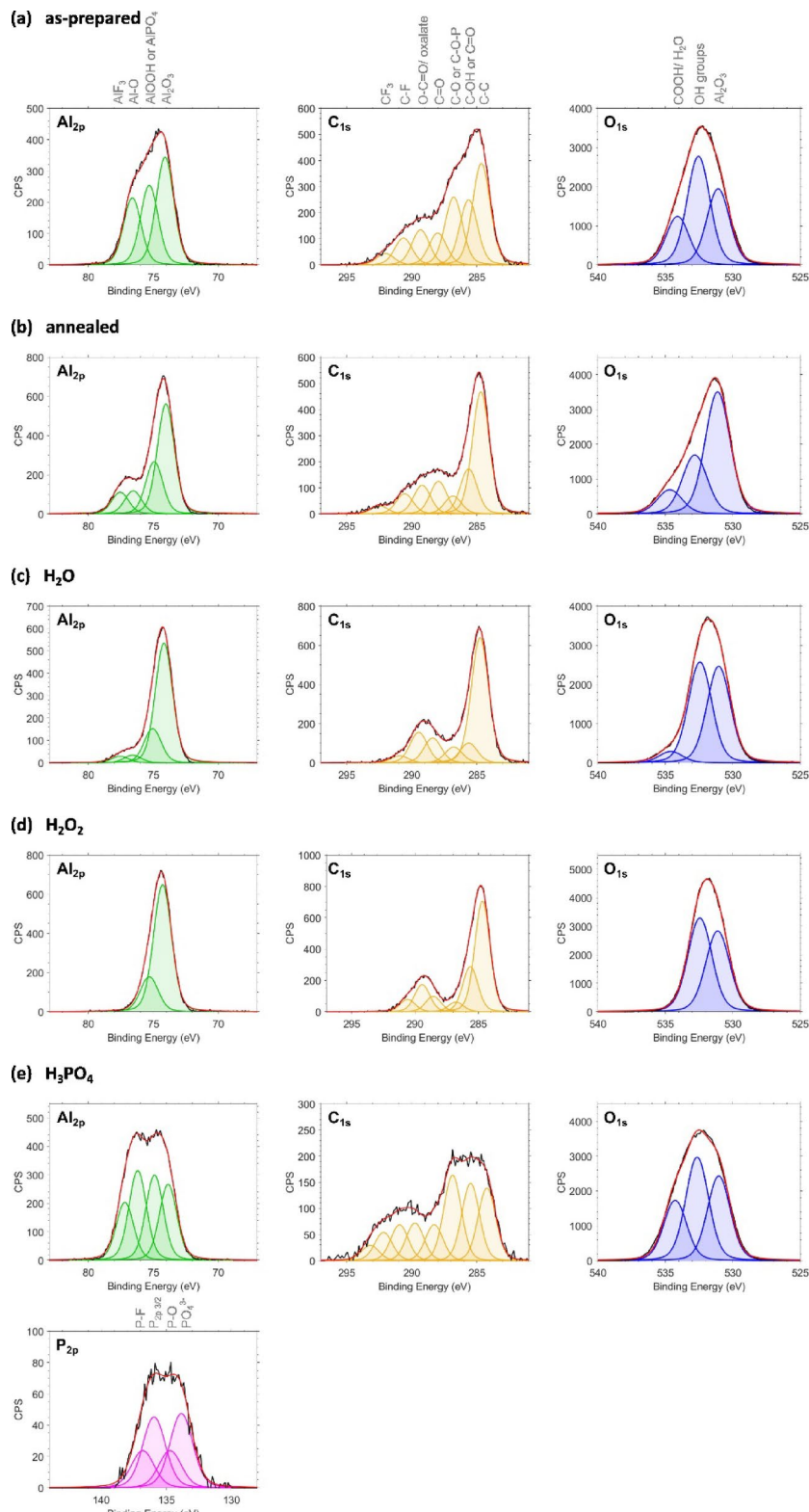


Fig. 4. XPS measurements reveal the influence of different post-anodization treatments on the surface chemistry of AAO templates. The AAO templates are (a) as-prepared, (b) annealed at 450 °C for 1 h, (c) exposed to H_2O for 24 h, (d) immersed into 30 wt% H_2O_2 for 24 h followed by H_2O for 24 h, and (e) soaked into 5 wt% H_3PO_4 for 1 min.

a low standard deviation. Moreover, no additional washing out of electrolyte ions can occur because the ions are already removed, decomposed, or saturated after the post-anodization treatment with an H_2O_2 -containing aqueous solution.

H_3PO_4 is often applied for pore-widening of AAO templates by etching alumina^{18,19}. During the alumina dissolution, this etching process simultaneously releases the incorporated electrolyte species from the structure¹⁸. Since aluminum ions are released into the solution by the etching, it is possible that they react with the dissolved electrolyte ions to form side-products such as aluminum oxalate. Figure 4e demonstrates decreasing peaks of O-C=O, C=O, and C-C/C-H bonds and a slight increase of the OH groups in the O_{1s} peak compared to the as-prepared sample. However, besides the hypothesized formation of Al-oxalate complexes, reactions of the phosphoric acid with Al ions are also possible. We assume that they result in the formation of Al-phosphate. Since the B.E.s for O=P, O-P, and Al-O-P groups (additional panel in Fig. 4e)) are similar to the aforementioned ones, it cannot be unambiguously distinguished. The Al_{2p} peak shows a similar ratio of both sub-peaks which was not observed for any of the other treatments. This might also be caused by the additional groups featuring similar binding energies, namely $AlPO_4$ similar to $Al(OOH)$. The additional P_{2p} peak also reveals the presence of phosphorus containing groups. Specifically, PO_4^{3-} and P-O-Al groups are detected. For samples immersed in H_3PO_4 , the proposed formation of phosphorus containing aluminum groups might reduce the overall photocatalytic activity due to changes in the dye adsorption at the AAO surface. Hence, these structures feature a lower mean activity after three photocatalysis measurements. However, the activity variation is even lower than for the H_2O_2 -treated sample which probably originates from stabilization of the surface chemistry by the formation of Al-phosphate groups. The surface chemistry alterations by the different treatments do not affect the morphology of the AAO templates as demonstrated by cross-section SEM images (Figure S7). Moreover, the pore morphology is not altered during the photocatalysis measurement. This is also exemplarily shown by top-view SEM images of the H_2O_2 -treated AAO template (Figure S8).

The photocatalysis measurements of the ALD-functionalized AAO templates presented in Fig. 2 can also be well explained by the results from the XPS study. TiO_2 -coating of as-prepared and post-anodization surface-modified AAO samples show stable photocatalytic activities over three measurements. The variations between the first and third measurements are very small and all tested templates benefit from the TiO_2 functionalization by exhibiting increased photocatalytic activities compared to the uncoated counterparts depicted in Fig. 3. In detail, the TiO_2 coating improved the photocatalytic performances by up to 12%. Note, the small increase in photocatalytic activity after TiO_2 coating is associated with the utilized light source which emits mostly visible radiation that is not suitable to excite TiO_2 . The ratio of the photocatalytic performances when comparing the individual treatments remains constant – as-prepared and H_2O_2 -modified templates demonstrate similar photocatalytic activities, but the H_3PO_4 -treated sample shows a lower activity. This is in good agreement with the high chemical stability of TiO_2 ³⁷. Similarly, the constant photocatalytic activities of H_2O_2 - and H_3PO_4 -treated AAO templates are maintained after Fe_2O_3 functionalization. In contrast, as-prepared templates coated with Fe_2O_3 show decreasing activities over consecutive measurements. The activity decrease might be caused by the reaction of electrolyte ions in the as-prepared AAO structure with Fe_2O_3 when activated by charge carriers during the photocatalytic processes. This could induce chemical modification of Fe_2O_3 at the interface to the AAO template which could result in an activity decline over multiple measurements. Consequently, improving the chemical stability of the templates' surface is beneficial for studying chemically less stable photocatalysts such as Fe_2O_3 . Note that depositing Fe_2O_3 onto AAO templates modified with H_3PO_4 significantly boosts the photocatalytic performance compared to functionalizing a H_3PO_4 -treated AAO template with TiO_2 . We believe that coating Fe_2O_3 onto the treated AAO template might not only result in the growth of Fe_2O_3 , but might also lead to the formation of iron phosphate or iron hydroxy phosphate compounds based on the presence of phosphate groups at the interface between the surface modified AAO template and the ALD prepared Fe_2O_3 layer^{48–50}. These materials also exhibit good photocatalytic activities as identified by previous studies^{48–53}. Local formation of iron phosphate or iron hydroxy phosphate at the AAO/ Fe_2O_3 interface might explain the significant performance increase when H_3PO_4 -treated AAO templates are functionalized with Fe_2O_3 instead of TiO_2 .

Conclusion

To sum up, post-anodization treatments of AAO templates modify their surface chemistry as revealed by XPS measurements. We found that functional groups originating from electrolyte ions incorporated into the AAO matrix during anodization can be reduced by different treatments. Specifically, the Al-OOH and Al-O groups as well as C=O are decreased while the Al_2O_3 content increased. Modifications of the surface chemistry by the tested treatments determine the photocatalytic behavior of the respective AAO template structures. Especially the stability of the photocatalytic activity over consecutive measurements can be enhanced when aqueous solutions containing H_2O_2 or H_3PO_4 are utilized. Functionalizing post-anodization modified AAO templates with TiO_2 results in stable photocatalytic performances over consecutive measurements, because TiO_2 itself is a chemically very stable material. Thus, it is not influenced by the surface chemistry of the underlying AAO template. Contrary, the photocatalytic stability of AAO templates functionalized with Fe_2O_3 – as a chemically less stable photocatalyst – is significantly affected by the post-anodization treatment. These results could assist the characterization of new functional materials in the future by employing chemically stable nanostructured templates, such as post-anodization modified AAO.

Methods

Materials

Aluminum (Al) chips (99.9997%, 0.05 mm thickness, 2 cm diameter) were received from Goodfellow GmbH (Germany). Perchloric acid ($HClO_4$, CAS 7601-90-3), ethanol (C_2H_5OH , EtOH, CAS 64-17-5), isopropyl

alcohol (C_3H_8O , IPA, CAS 67-63-0), oxalic acid ($H_2C_2O_4$, CAS 144-62-7), chromium (VI) oxide (CrO_3 , CAS 1333-82-0), phosphoric acid (H_3PO_4 , CAS 7664-38-2), hydrochloric acid (HCl, CAS 7647-01-0), copper (II) chloride dihydrate ($CuCl_2 \cdot 2 H_2O$, CAS 10125-13-0), methylene blue ($C_{16}H_{18}ClN_3S$, MB, CAS 122965-43-9), hydrogen peroxide (H_2O_2 , CAS 7722-84-1), and titanium tetraisopropoxide (TTIP, CAS 546-68-9) were purchased from Sigma Aldrich (Germany) and used as received. Milli-Q water ($> 16 M\Omega \text{ cm}$, H_2O) was utilized as ALD precursor and to prepare aqueous solutions. Ferrocene ($C_{10}H_{10}Fe$, Cp_2Fe , CAS 102-54-5) was supplied by Alfa Aesar (Germany) and trimethylaluminum (C_3H_9Al , TMA, CAS 75-24-1) was purchased from Strem Chemicals (France). Nitrogen (6.0) and oxygen (5.0) were supplied by SOL (Germany) and Westfalen (Germany), respectively.

Fabrication of AAO

AAO templates were produced by two-step anodization of aluminum. Prior to anodization, the Al chips were cleaned by immersion in IPA and H_2O for 30 min, respectively, and were dried under nitrogen stream. The cleaned chips were electropolished in a $HClO_4/EtOH$ solution (1:4, v: v) at 20 V and 5 °C for 3 min. The first anodization step was conducted in aqueous $H_2C_2O_4$ (0.3 M) at 40 V and 6 °C for 20 h. Afterwards, the formed nanoporous Al_2O_3 film was removed by etching in aqueous H_2CrO_4/H_3PO_4 solution (1.8 wt% / 6 wt%) at 45 °C for 24 h. The second anodization step was conducted under the same conditions as the first one except the duration which was set to 10 h.

Surface modification of AAO

Subsequent to the anodization, AAO templates were treated by different surface modification approaches while one sample was kept as-prepared without further treatment as reference. The surface treatments were as follows: (i) heat: annealed at 450 °C on a hotplate for 1 h in ambient atmosphere; (ii) polar solvent: immersed into H_2O for 24 h and afterwards dried with N_2 stream; (iii) chemical type I: immersed into H_2O_2 (30 wt%) for 24 h and H_2O for another 24 h before it was dried under N_2 stream; (iv) chemical type II: immersed into H_3PO_4 (5 wt%) at 45 °C for 1 min, rinsed and dried with a N_2 stream. Annealing at 600 °C for 1 h was conducted in ambient atmosphere in a rapid thermal annealing oven OTF-1200X-4-RTP (MTI Corporation, USA). The heating rate was 5 °C/s and the base pressure was set to 200 Torr.

For functionalizing AAO templates with a photocatalyst, one as-prepared sample, one sample immersed in H_2O_2 (30 wt%) for 24 h and H_2O for 24 h, and one sample exposed to H_3PO_4 for 1 min were coated with TiO_2 or Fe_2O_3 and an ultra-thin Al_2O_3 protection layer by ALD, respectively. TiO_2 coating was conducted in a GEMStar XT[™] (Arradiance, USA) ALD reactor under stop-flow conditions at 150 °C and a N_2 carrier gas flow of 30 sccm. TTIP heated to 80 °C and H_2O at room temperature were pulsed for 0.1 s and 0.05 s, respectively. Exposure and purge times of 60 s and 120 s were applied for both half reactions. 96 cycles were applied to obtain a TiO_2 thickness of 5 nm. Cp_2Fe at 100 °C and O_3 at room temperature were used as precursors in the Fe_2O_3 process which was operated in stop-flow mode at 200 °C in a home-built ALD system. Each Cp_2Fe half-cycle consisted of 2 s precursor pulse, 60 s exposure, and 90 s pumping of the system. The O_3 half-cycle was repeated twice within one complete ALD cycle and 0.08 s precursor pulse, 30 s exposure, and 90 s pump time were applied. Each sample was exposed to 179 cycles for Fe_2O_3 deposition resulting in a coating thickness of 5 nm. Subsequently, the samples were coated with an ultra-thin film of Al_2O_3 as protection layer to prevent photocorrosion of the Fe_2O_3 film³⁸. Al_2O_3 deposition was conducted in stop-flow mode at 150 °C using TMA and H_2O (both at room temperature) as precursors. Both half-cycles consisted of 0.05 s precursor pulse, 60 s exposure, and 90 s pumping. The samples were coated by 2 cycles of Al_2O_3 .

Composition and structural analysis of modified AAO

XPS measurements were conducted in a Theta Probe XPS instrument (Thermo Fisher Scientific Inc., USA) and the XPS data analysis was performed using the CasaXPS software package. A pass energy of 50 eV and 200 eV and a step size of 0.1 eV and 0.5 eV were applied for core level scans and survey spectra, respectively. XPS spectra calibration was based on the C-C component in the C1s XPS spectrum at 284.8 eV. The XPS spectra were deconvoluted by fitting a Shirley background and symmetric Voigt function which is listed for each sample in Table S3. EDX measurements were conducted with a Crossbeam 550 scanning electron microscope (Zeiss, Germany) at an applied voltage of 15 kV. SEM images were acquired with the Zeiss Crossbeam 550 SEM at an applied voltage of 2 kV and a current of 10 pA. Prior to taking cross-section SEM images, the Al backsides of the AAO templates were removed by etching in a saturated $CuCl_2/HCl$ solution by defining the Al area with a Kapton mask featuring a circular hole at the AAO position.

Photocatalytic characterization

Photocatalytic characterization was carried out by analyzing the photocatalytic degradation of methylene blue (MB) as a model pollutant of water. A sample was mounted into a home-built photocatalysis cell composed of polyether ether ketone (PEEK) and a soda-lime glass window. The sample was exposed to a MB solution (2.5 mg l^{-1} , 8 ml) which also contained H_2O_2 (200 mM) and kept in darkness for one hour to establish the adsorption-desorption equilibrium of the molecules at the samples surface. Subsequently, the system was irradiated with UV-visible light generated by an Euromex LE.5211 lamp equipped with a Philips 64,230 FO halogen bulb. The absorbance of the dye solution was analyzed every five minutes by UV/Vis spectroscopy. For this, 1 ml of the MB solution was pipetted from the photocatalysis cell into a cuvette, analyzed in the spectrometer, and pipetted back. During that time, illumination of the photocatalysis cell was blocked to prevent degradation within this analysis period. Lambert-Beer's law was applied to calculate the MB concentration based on the measured absorbance at every point in time. The photocatalytic reaction is assumed to occur *via* the Langmuir-Hinshelwood mechanism.

Since the MB concentration is lower than 10^{-3} mol l⁻¹, the reaction rate can be simplified to a pseudo-first-order kinetics law:

$$\ln \left(\frac{c}{c_0} \right) = -k \cdot t$$

Here, c denotes the concentration of the MB solution at a given time t , c_0 describes the concentration at the beginning of the measurement ($t=0$ h), and k is the apparent photocatalytic rate constant which is a measure for the photocatalytic activity of a sample. The photocatalytic MB degradation measurement was repeated three times per sample to monitor changes of the activity over consecutive measurements.

Data availability

The datasets generated during and/or analyzed during the current study are available from the corresponding author on reasonable request.

Received: 20 January 2025; Accepted: 14 April 2025

Published online: 29 April 2025

References

1. Chaikittisilp, W., Yamauchi, Y. & Ariga, K. Material evolution with nanotechnology, nanoarchitectonics, and materials informatics: what will be the next paradigm shift in nanoporous materials? *Adv. Mater.* **34**, 2107212 (2022).
2. Benelmekki, M. *Nanomaterials the Original Product of Nanotechnology* (Morgan & Claypool, 2019).
3. Kumar, N. & Kumbhat, S. *Essentials in Nanoscience and Nanotechnology* (John Wiley & Sons Inc., 2016).
4. Ibadon, A. O. & Fitzpatrick, P. Heterogeneous photocatalysis: recent advances and applications. *Catalysts* **3**, 189–218 (2013).
5. Beydoun, D., Amal, R., Low, G. & McEvoy, S. Role of nanoparticles in photocatalysis. *J. Nanoparticle Res.* **1**, 439–458 (1999).
6. Md Jani, A. M., Lasic, D. & Voelcker, N. H. Nanoporous anodic aluminium oxide: advances in surface engineering and emerging applications. *Prog Mater. Sci.* **58**, 636–704 (2013).
7. Lim, S. Y. et al. Nanoporous anodic alumina photonic crystals for sunlight harvesting applications: A perspective. *Sol RRL* **2200480** <https://doi.org/10.1002/solr.202200480> (2022).
8. Lim, S. Y. et al. Electrochemical engineering of nanoporous materials for photocatalysis: fundamentals, advances, and perspectives. *Catalysts* **9**, 988 (2019).
9. Jing, L., Zhou, W., Tian, G. & Fu, H. Surface tuning for oxide-based nanomaterials as efficient photocatalysts. *Chem. Soc. Rev.* **42**, 9509–9549 (2013).
10. Sapoletova, N. A. et al. Effect of post-treatment on photocatalytic activity of anodic Titania photonic crystals. *Opt. Mater.* **144**, 114350 (2023).
11. Santos, A., Kumeria, T. & Lasic, D. Nanoporous anodic aluminum oxide for chemical sensing and biosensors. *TrAC - Trends Anal. Chem.* **44**, 25–38 (2013).
12. Kumeria, T., Santos, A. & Lasic, D. Nanoporous anodic alumina platforms: engineered surface chemistry and structure for optical sensing applications. *Sens. Switz.* **14**, 11878–11918 (2014).
13. Lee, W. & Park, S. J. Porous anodic aluminum oxide: anodization and templated synthesis of functional nanostructures. *Chem. Rev.* **114**, 7487–7556 (2014).
14. Santos, A. Nanoporous anodic alumina photonic crystals: fundamentals, developments and perspectives. *J. Mater. Chem. C.* **5**, 5581–5599 (2017).
15. Masuda, H. & Fukuda, K. Ordered metal nanohole arrays made by a Two-Step replication of honeycomb structures of anodic alumina. *Science* **268**, 1466–1468 (1995).
16. Lv, Y. Research progress in formation of anodizing aluminum oxide. *IOP Conf. Ser. Earth Env Sci.* **8**, 68–74 (2017).
17. Le Coz, F., Arurault, L. & Datas, L. Chemical analysis of a single basic cell of porous anodic aluminium oxide templates. *Mater. Charact.* **61**, 283–288 (2010).
18. Han, H. et al. In situ determination of the pore opening point during wet-chemical etching of the barrier layer of porous anodic aluminum oxide: nonuniform impurity distribution in anodic oxide. *ACS Appl. Mater. Interfaces.* **5**, 3441–3448 (2013).
19. Santos, A., Kumeria, T., Wang, Y. & Lasic, D. In situ monitored engineering of inverted nanoporous anodic alumina funnels: on the precise generation of 3D optical nanostructures. *Nanoscale* **6**, 9991–9999 (2014).
20. Xu, D., Zhen, C. & Zhao, H. Microstructure and photoluminescence properties of anodized aluminum oxide films treated by argon ion. *Ceram. Int.* **47**, 14382–14389 (2021).
21. Gopal Khan, G., Singh, A. K. & Mandal, K. Structure dependent photoluminescence of nanoporous amorphous anodic aluminium oxide membranes: role of F⁺ center defects. *J. Lumin.* **134**, 772–777 (2013).
22. Li, G. H., Zhang, Y., Wu, Y. C. & Zhang, L. D. Wavelength dependent photoluminescence of anodic alumina membranes. *J. Phys. Condens. Matter.* **15**, 8663–8671 (2003).
23. Gao, T., Meng, G. & Zhang, L. Blue luminescence in porous anodic alumina films: the role of the oxalic impurities. *J. Phys. Condens. Matter.* **15**, 2071–2079 (2003).
24. Han, Y. et al. Quantitative investigation in the influence of oxalic impurities on photoluminescence properties of porous AAOs. *Mater. Chem. Phys.* **129**, 1247–1251 (2011).
25. Li, G. H., Zhang, Y., Wu, Y. C. & Zhang, L. D. Photoluminescence of anodic alumina membranes: pore size dependence. *Appl. Phys. Mater. Sci. Process.* **81**, 627–629 (2005).
26. Karunakaran, C., Magesan, P., Gomathisankar, P. & Vinayagamoorthy, P. Photocatalytic degradation of dyes by Al₂O₃–TiO₂ and ZrO₂–TiO₂ nanocomposites. *Mater. Sci. Forum.* **734**, 325–333 (2013).
27. Araoyinbo, A. O., Derman, M. N. & Rahmat, A. Rafezi Ahmad, K. Organic dye degradation with TiO₂ Catalyst/AAO template in the presence of H₂O₂. *Adv. Mater. Res.* **795**, 649–653 (2013).
28. Zhang, J., Tian, B., Wang, L. & Xing, M. *Photocatalysis Fundamentals, Materials and Applications* (Springer Open Ltd, 2018).
29. Ahmed, S. N. & Haider, W. Heterogeneous photocatalysis and its potential applications in water and wastewater treatment: A review. *Nanotechnology* **29**, (2018).
30. Fox, M. A. & Dulay, M. T. Heterogeneous photocatalysis. *Chem. Rev.* **93**, 341–357 (1993).
31. Mills, A. & Le Hunte, S. An overview of semiconductor photocatalysis. *J. Photochem. Photobiol. Chem.* **108**, 1–35 (1997).
32. Herrmann, J. M. Heterogeneous photocatalysis: fundamentals and applications to the removal of various types of aqueous pollutants. *Catal. Today* **53**, 115–129 (1999).
33. George, S. M. Atomic layer deposition: an overview. *Chem. Rev.* **110**, 111–131 (2010).
34. Bae, C., Shin, H. & Nielsch, K. Surface modification and fabrication of 3D nanostructures by atomic layer deposition. *MRS Bull.* **36**, 887–897 (2011).

35. Knez, M., Nielsch, K. & Niinistö, L. Synthesis and surface engineering of complex nanostructures by atomic layer deposition. *Adv. Mater.* **19**, 3425–3438 (2007).
36. Cremers, V., Puurunen, R. L. & Dendooven, J. Conformality in atomic layer deposition: current status overview of analysis and modelling. *Appl. Phys. Rev.* **6**, 021302 (2019).
37. Zhang, Y. et al. Titanate and Titania nanostructured materials for environmental and energy applications: A review. *RSC Adv.* **5**, 79479–79510 (2015).
38. Hedrich, C. et al. Enhancing the photocatalytic activity by tailoring an anodic aluminum oxide photonic crystal to the semiconductor catalyst: at the example of Iron oxide. *Adv. Mater. Interfaces.* **10**, 2300615 (2023).
39. Biesinger, M. C. et al. Quantitative chemical state XPS analysis of first row transition metals, oxides and hydroxides. *J. Phys. Conf. Ser.* **100**, 012025 (2008).
40. Biesinger, M. C., Lau, L. W. M., Gerson, A. R. & Smart, R. St. C. Resolving surface chemical States in XPS analysis of first row transition metals, oxides and hydroxides: Sc, Ti, V, Cu and Zn. *Appl. Surf. Sci.* **257**, 887–898 (2010).
41. Hughes, A. E., Easton, C. D., Gengenbach, T. R., Biesinger, M. C. & Laleh, M. Interpretation of complex x-ray photoelectron peak shapes. II. Case study of Fe 2p3/2 fitting applied to austenitic stainless steels 316 and 304. *J. Vac Sci. Technol. A.* **42**, 053206 (2024).
42. Li, J. & Wu, N. Semiconductor-based photocatalysts and photoelectrochemical cells for solar fuel generation: A review. *Catal. Sci. Technol.* **5**, 1360–1384 (2015).
43. Weng, B., Qi, M., Han, C., Tang, Z. & Xu, Y. Photocorrosion Inhibition of Semiconductor-Based photocatalysts: basic principle, current development, and future perspective. *ACS Catal.* **9**, 4642–4687 (2019).
44. Chen, S. et al. Semiconductor-based photocatalysts for photocatalytic and photoelectrochemical water splitting: will we stop with photocorrosion? *J. Mater. Chem. Mater. Energy Sustain.* **8**, 2286–2322 (2020).
45. Monteiro, M. C. O., Schmuki, P. & Killian, M. S. Tuning anatase surface reactivity toward carboxylic acid anchor groups. *Langmuir* **33**, 13913–13922 (2017).
46. Trochowski, M. et al. How insignificant modifications of photocatalysts can significantly change their photocatalytic activity. *J. Mater. Chem. A.* **7**, 25142–25154 (2019).
47. Chung, D. Y. et al. Decomposition of oxalate by hydrogen peroxide in aqueous solution. *J. Radioanal Nucl. Chem. Lett.* **201**, 495–507 (1995).
48. Guo, W., Cao, Y., Zhang, Y., Wang, L. & Kong, L. Synthesis of porous iron hydroxy phosphate from phosphate residue and its application as a Fenton-like catalyst for dye degradation. *J. Environ. Sci.* **112**, 307–319 (2022).
49. Zhang, Y. et al. Eco-friendly ferrocene-functionalized Chitosan aerogel for efficient dye degradation and phosphate adsorption from wastewater. *Chem. Eng. J.* **439**, 135605 (2022).
50. Arshadi, M., Zandi, H., Akbari, J. & Shamsi, A. Ferrocene functionalized nanoscale mixed-oxides as a potent phosphate adsorbent from the synthetic and real (Persian Gulf) waters. *J. Colloid Interface Sci.* **450**, 424–433 (2015).
51. Yu, D. et al. Structural and catalytic investigation of mesoporous Iron phosphate. *J. Phys. Chem. C.* **111**, 14394–14399 (2007).
52. Wagh, A. S. & Jeong, S. Y. Chemically bonded phosphate ceramics: III, reduction mechanism and its application to Iron phosphate ceramics. *J. Am. Ceram. Soc.* **86**, 1850–1855 (2003).
53. Mimouni, I. et al. Iron phosphate for photocatalytic removal of ibuprofen from aqueous media under sun-like irradiation. *J. Photochem. Photobiol. Chem.* **433**, 114170 (2022).

Acknowledgements

The authors gratefully acknowledge the financial support from the Deutsche Forschungsgemeinschaft (DFG, German Research Foundation)–Projektnummer 192346071–SFB 986, from TUHH’s internal funding support HEXC312003 “BlueMat”, and from the special research fund BOF of Ghent University (BOF-GOA, 01G01019). We acknowledge the use of the Hamburg-CRR cleanroom facility, jointly operated by UHH, DESY, and MPSD, which was instrumental for the work presented in this paper. Further, we acknowledge financial support from the Open Access Publication Fund of Universität Hamburg.

Author contributions

C. H.: conceptualization; methodology; data curation; formal analysis and visualization; validation; writing original draft; writing-review & editing. R. R. P.: data curation; formal analysis and visualization; validation; writing-review & editing. M. M. M.: data curation; formal analysis and visualization; validation; writing-review & editing. A. R. B.: data curation; formal analysis and visualization; writing-review & editing. S. H.: data curation; formal analysis and visualization; writing-review & editing. K. P. F.: validation; project administration; supervision; funding acquisition and resources; writing-review & editing. C. D.: methodology; validation; project administration; supervision; funding acquisition and resources; writing-review & editing. J. D.: methodology; validation; project administration; supervision; funding acquisition and resources; writing-review & editing. R. H. B.: validation; project administration; supervision; funding acquisition and resources; writing-review & editing. R. Z.: conceptualization, methodology, validation; project administration; supervision; funding acquisition and resources; writing-review & editing.

Funding

Open Access funding enabled and organized by Projekt DEAL.

Declarations

Competing interests

The authors declare no competing interests.

Additional information

Supplementary Information The online version contains supplementary material available at <https://doi.org/10.1038/s41598-025-98635-3>.

Correspondence and requests for materials should be addressed to R.Z.

Reprints and permissions information is available at www.nature.com/reprints.

Publisher's note Springer Nature remains neutral with regard to jurisdictional claims in published maps and institutional affiliations.

Open Access This article is licensed under a Creative Commons Attribution 4.0 International License, which permits use, sharing, adaptation, distribution and reproduction in any medium or format, as long as you give appropriate credit to the original author(s) and the source, provide a link to the Creative Commons licence, and indicate if changes were made. The images or other third party material in this article are included in the article's Creative Commons licence, unless indicated otherwise in a credit line to the material. If material is not included in the article's Creative Commons licence and your intended use is not permitted by statutory regulation or exceeds the permitted use, you will need to obtain permission directly from the copyright holder. To view a copy of this licence, visit <http://creativecommons.org/licenses/by/4.0/>.

© The Author(s) 2025